Song et al., J Nucl Ene Sci Power Generat Technol 2017, 6:4
DOI: 10.4172/2325-9809.1000178

Journal of Nuclear Energy Science & Power Generation Technology

Research Article

A SCITECHNOL JOURNAL

Influence of Aluminum Addition on the Corrosion of 304 Stainless Steel in High Temperature Water

Xiao-Fang Song*, Sheng-Han Zhang and Ke-Gang Zhang

Abstract

The influence of Al^{3+} addition on the corrosion of 304 stainless steel (SS) in high temperature water has been investigated by gravimetric analysis, potentiodynamic polarization and Mott-Schottky plots. After Al^{3+} addition, the amount of oxidized metal on 304 SS was reduced, the open circuit potential was shifted towards positive direction, the passive current density was declined, and the donor density of the oxide film formed on 304 SS surface was decreased. The corrosion kinetics of 304 SS in this work was curved to be parabolic with a 25% reduction of the parabolic rate constant by Al^{3+} addition. The activation energy of the corrosion process was increased due to the presence of Al which slowed down the 304 SS corrosion. The structure and composition of oxide film formed on 304 SS in high temperature water may be changed by Al^{3+} addition. The work may give a decent route for radiation field or consumption control in the essential circuit water of PWR.

Keywords

Aluminum addition; 304 Stainless steel; Pressurized water reactor; Corrosion kinetics; Oxide film

Introduction

A 304 stainless steel (SS) has been widely used as structural material in many nuclear power plants for its excellent mechanical properties, especially for its corrosion resistance. In general, the corrosion rate of 304 SS in nuclear reactor coolant system is very slow. Even so, the transmitting and activation of corrosion products must be taken seriously [1,2]. The presence of ^{60}Co in the primary circuit water of pressurized water reactor (PWR) is one primary cause which aggravates the corrosion of material and radiation build-up. Zn addition technology was often used for radiation field and corrosion control, which may change the composition and structure of oxide film formed on 304 SS [3,4]. ^{60}Co in the spinel oxides formed on stainless steel may be replaced by Zn^{2+}, which may reduce the corrosion speed of 304 SS and the dose rate of Co [5]. However, natural zinc could be activated into ^{65}Zn which may also result in radiation build-up [6]. Along these lines, the costly drained Zinc rather than regular zinc was utilized which implies a much high cost. Some ease innovation is required for the erosion and radiation develop control in Nuclear power plants. Aluminum (Al3+) expansion might be a decent decision which can diminish the consumption of the 304 SS and 316 SS in the bubbling water reactor (BWR) essential coolant while the normal Al isotopes won't bring about the radiation field develop [7]. In this study, the influence of Al^{3+} addition on the corrosion behavior of 304 SS has been investigated in the simulated primary circuit water of pressurized water reactor (PWR).

Experimental

Materials

The chemical composition of the 304 SS used in the present work was listed as follows (wt, %): 0.045 C, 0.63 Si, 1.10 Mn, 8.06 Ni, 19.57 Cr and balance Fe. The 304 SS specimens (12 mm ×10 mm × 2 mm) were mechanically ground in turn with 400, 600, 800, 1200, 1500 and 2000-grit silicon carbide papers and then mechanically polished with alumina gel (0.5 μm). The specimens were ultrasonically cleaned by ethanol and pure water in sequence. Then the specimens were dried with cold wind and then measured for the precise dimension and weight. All the specimens were kept in the dry vessel for use.

Exposure Tests

The specimens were exposed in the simulated primary circuit water of PWR contained in a 1 L stainless steel autoclave. The simulated solutions contained 1200 mg/L H_3BO_3 (counted as B), 2.2 mg/L $LiOH{\cdot}H_2O$ (counted as Li) and 2 mg/L $(CH_3COO)_2Co{\cdot}4H_2O$ (counted as Co, ^{59}Co instead of ^{60}Co) with or without 0.1 mg/L $(CH_3COO)_3Al$ (counted as Al). Before exposure, the aqueous solutions were deaerated by continuous bubbling with nitrogen gas for 2 h. Test specimens were exposed in the above aqueous environment at 473.15 K, 523.15 K and 553.15 K, respectively. The examples after introduction were cleaned and cooled, and afterward put away in the dry vessel for utilize.

Gravimetric analysis

The specimens (triplicate corrosion specimens) after exposure were descaled using a two-step alkaline permanganate/ammonium citrate process: (1) 3% $KMnO_4$ and 10% NaOH for 5 min boiling followed by wiping and (2) 10% $(NH_4)_2HC_6H_5O_7$ for 5 min boiling. This ideal descaling arrangement was dictated by analyze and the strategy for concoction descaling alludes to ASTM G1-03. The descaled examples were ultrasonically cleaned by ethanol and unadulterated water. The specimens were all dried to a constant weight. The descaled weight-loss of 304 SS specimen was calculated by Eq. 1:

$$\Delta w = \frac{w_0 - w_1}{S} \quad (1)$$

Here, w_0 is the weight of specimen before exposure (mg), w_1 is the weight of specimen after descaling (mg), and S is the superficial area of the specimen (dm^2).

Electrochemical measurements

The electrochemical experiments were carried out by a classical three-electrode cell. A platinum counter electrode and a saturated calomel reference electrode (SCE, all potential values mentioned refer to) were employed in the three-electrode cell. The exposed specimens were used as the working electrode which was encapsulated by polytetrafluoroethylene (PTFE) tape with a 0.2826 cm^2 window

***Corresponding author:** Xiao-Fang Song, School of Environmental Science & Engineering, North China Electric Power University, Baoding 071003, Hebei Province, P. R. China, Tel: +86-312-7525535; Fax: +86-312-7525535; E-mail: wantong1998@163.com

Received: October 30, 2017 **Accepted:** November 08, 2017 **Published:** November 15, 2017

exposed. Fresh exposed specimen was used in each electrochemical experiment. All measurements were performed at room temperature in the borate buffer solutions (0.15 mol/L boric acid, 0.0375 mol/L sodium borate, pH=8.4) with Parstat 2273.

Potentiodynamic polarization and Mott-Schottky plots were utilized to examine electrochemical attributes of oxide films on 304 SS after high temperature presentation. The potentiodynamic polarization tests were performed at 1 mV/s checking rate. The capacitance experiments (Mott-Schottky plots) were performed at 1 kHz frequency and with 10 mV intervals in the potential range from 0.2 to -0.4V.

Results and Discussion

Gravimetric analysis

Table 1 summarizes the amounts of descaled weight losses on 304 SS specimens after exposure. The descaled weight loss of 304 SS specimen represents the total amount of the oxidized metals on 304 SS. It shows that the weight loss (oxidized metal) of 304 SS increases significantly with the temperature increases. It indicates that the corrosion resistance of 304 SS decreases in high temperature solution. It must be illustrated that weight loss of 304 SS is reduced by Al^{3+} addition into the simulated solution. This indicates that Al^{3+} addition reduces the oxidation of 304 SS and strengthens its corrosion resistance.

Figure 1 shows the weight loss on 304 SS specimen along with exposure time before and after Al^{3+} addition. The measure of oxidized metals in the underlying stage expanded forcefully which exhibits the core arrangement of oxide at the deformities of 304 SS. At that point, the expansion of oxidized metals was backed off in the center and later stages demonstrating the arrangement of an entire oxide film. The primary quick back moderate erosion rate shows the change of consumption conduct from substance response control to dissemination process control. Corrosion kinetics of 304 SS was analyzed according to the weight loss of the original specimen (Δw) accompanied by the increasing of exposure time (Figure 1).

The corrosion kinetics was fitted to the parabolic model under all reaction conditions. The corrosion kinetics can be curved by Eq. 2

$$\Delta w = k_p t^{0.5} \quad (2)$$

Here, k_p is the parabolic rate constant (mg metals·dm^{-2}·h$^{-0.5}$) and t is the reaction time (h). The parabolic rate at each temperature was calculated showing an increase with temperature as happened in most chemical reactions. The fitted parabolic rate constants of 304 SS exposed at 473.15, 523.15 and 553.15 K in Al-free simulated solutions are 0.862, 1.265 and 1.360 mg metals·dm^{-2}·h$^{-1/2}$, respectively (Figure 1a). Remarkably, the fitted parabolic rate constants of 304 SS exposed at 473.15, 523.15 and 553.15K in Al-containing simulated solutions are lowered to 0.633, 0.939 and 1.085 mg metals·dm^{-2}·h$^{-1/2}$, respectively (Figure 1b). The results show a significant decrease in the parabolic rate constant (about 25%) due to presence of Al^{3+}. Such phenomenon gives a direct evidence for the inhibition behavior by Al^{3+} in corrosion process of 304 SS.

The Arrhenius equation is an empirical formula used in the chemical process to indicate the relationship between the reaction rate constant and the temperature change. The activation energy can be obtained by the logarithmic expression of Arrhenius equation:

$$\ln k = -E_a / RT + \ln A \quad (3)$$

Here, k is the corrosion reaction rate constant, R is the molar gas constant, E_a is the apparent activation energy of the reaction, T is the thermodynamic temperature, and A is the frequency factor. E_a is the

Table 1: Weight loss of 304 SS specimens exposed in various simulated solutions.

Time [h]	Δw [mg·dm^{-2}]					
	473.15[K]		523.15 [K]		553.15 [K]	
	Al_f[a]	Al_c[b]	Al_f	Al_c	Al_f	Al_c
24	-	-	-	-	8.8796	2.490
48	7.821	4.560	8.681	6.274	-	-
72	-	-	-	-	10.686	3.294
120	9.960	8.385	13.838	10.716	20.020	11.831
168	10.444	9.070	16.468	11.940	19.966	14.214

[a], Al-free solution; [b], Al-containing solution.

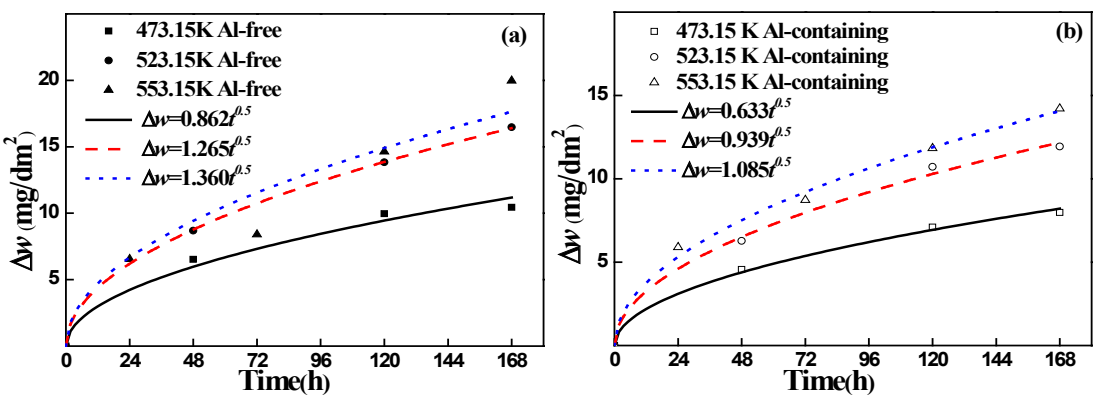

Figure 1: Oxidized metal of 304 SS exposed at 473.15K, 523.15K and 553.15K in various simulated solutions. (a) Al-free solution, (b) Al-containing solution.

energy needed when a reactant molecule transforms into a corrosion product. Hence, activation energy in the whole general corrosion process is introduced as a sensitivity indicator for initiation of corrosion on 304 SS under different temperatures. E_a can be calculated according to the slope of the plot of *lnk* versus *1/T*. The slope values are listed in Table 2. It shows that the activation energy of 304 SS in corrosion process is increased by Al addition, and the corrosion of 304 SS is slowed down. The relatively low values of activation energy may be attributed to the comparatively high temperature that used in this research (473.15-553.15K). It likewise might be clarified by that recurrence factor overwhelms the erosion rate when the consumption is controlled by dispersion process. At that point, the expansion of oxidized metals was backed off in the center and later stages demonstrating the arrangement of an entire oxide film. The primary quick back moderate erosion rate shows the change of consumption conduct from substance response control to dissemination process control [8]. The aluminum ions addition may change the structure of the oxide film formed on 304 SS which blocks the micropore diffusion of the metal ions.

Potentiodynamic polarization

Figure 2 shows the potentiodynamic polarization curves of the 304 SS specimens after 168 h exposure in the Al-free and Al-containing solutions. No obvious passivation range was observed and the anodic current density increases continuously with the increase of potential for the 304 SS specimens exposed in the Al-free simulated solution at 523.15 and 553.15K. However, the passive current density is remarkably reduced due to the presence of Al^{3+} at all temperatures. Specifically, the latent potential territory is clearly seen in the potentiodynamic polarization of the example uncovered in the Al-containing arrangement at 523.15 and 553.15K. These all indicates that the Al^{3+} addition in the simulated primary circuit water of PWR can strengthen the protection of 304 SS from corrosion.

Mott-Schottky plots

It is well established that corrosion performance of material is closely related with their semiconductor properties [9,10]. Semiconductor is highlighted by its low electron focus. At the point when a semiconductor is placed in a solution and the electron exchange between the two stages achieves equilibrium, a space charge layer (or an exhaustion layer) will be framed in favor of the oxide film in the interface district and a Helmholtz layer will be shaped in favor of the electrolyte. Under the fixed 1 *k*Hz frequency of Parstat 2273 in this experiment, the Helmholtz layer capacitance can be neglected and the measured capacitance is equal to the space charge layer capacitance [11,12]. The relationship between the space charge capacitance (C) and the applied potential (E) is obtained by the Mott-Schottky equation for n-type semiconductor (Eq.4):

$$\frac{1}{C^2} = \frac{2}{\varepsilon\varepsilon_0 e N_D}\left(E - E_{fb} - \frac{kT}{e}\right) \quad (4)$$

here ε is the dielectric constant of the oxide film, usually taken as, ε_0 is the vacuum permittivity (8.854×10^{-14} F/cm), e is the electron charge (1.602×10^{-19} C), N_D is the donor density, E_{fb} is the flat band potential, k is the Boltzmann constant (1.38×10^{-23} J/K), and T is the absolute temperature. N_D can be calculated from the slope of the C^{-2} versus E curve. Figure 3 shows the Mott-Schottky plots of 304 SS after high temperature exposure in Al-free and Al-containing simulated solutions [12,13]. The slopes of the curves are positive at the range of -0.4 - 0.1 V_{SCE}, suggesting an n-type semiconductor behavior of the oxide film on 304 SS. The N_D was calculated by the slope of the fitted lines, as shown in Table 3. The donor density increases with the increase of temperature indicating the weakened corrosion resistance [10, 14]. Interestingly, compared with the specimen exposed in Al-free solution, the donor density of the specimen exposed in Al-containing solution is decreased about 40% at each temperature. This suggests that the structure of oxide film can be changed by Al^{3+} addition which results in a stronger corrosion resistance.

Table 2: E_a of the corrosion process on 304 SS in the Al-free and Al-Containing solutions.

Solution	Slope	E_a [kJ/mol]
Al_f [a]	-1547.5	12.87
Al_c [b]	-1788.9	14.87

[a], Al-free solution; [b], Al-containing solution.

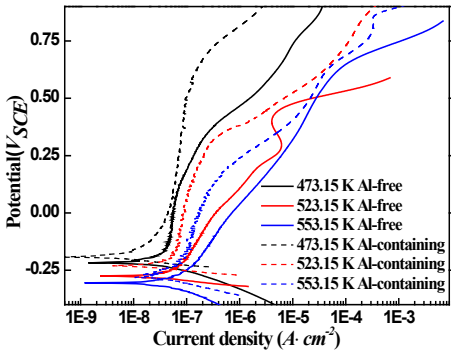

Figure 2: Potentiodynamic polarization curves of 304 SS specimen after 168 h exposure in various simulated solutions.

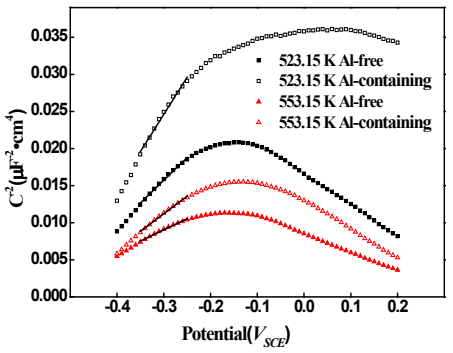

Figure 3: Mott-Schottky plots of the 304 SS specimen after 168 h exposure in various simulated solutions.

Table 3: Donor density of oxide films on 304 SS specimen after 168 h exposure in various simulated solutions.

	523.15 K Al_f [a]	523.15 K Al_c [b]	553.15 K Al_f [a]	553.15 K Al_c [b]
$N_D(cm^3)$	1.48×10^{20}	9.02×10^{19}	3.00×10^{20}	1.91×10^{20}

[a], Al-free solution; [b], Al-containing solution

Conclusions

The effect of Al^{3+} addition on the corrosion of 304 SS exposed to simulated primary circuit of PWR has been investigated by potentiodynamic polarization, Mott-Schottky plots and erosion energy. Al3+ expansion in high temperature water can diminish measure of the oxidized metal, bring down the consumption activity

vitality and change the semiconductor properties of the oxide film. Al^{3+} addition may change the structure of the oxide film formed on 304 SS. Al^{3+} addition will reduce the migration and activation of corrosion products by inhibiting the corrosion of the 304 SS in the primary circuit water of PWR. Al^{3+} water chemistry will be a good way to replace Zn water chemistry for radiation field and corrosion control.

References

1. Lin CC (2009) A review of corrosion product transport and radiation field buildup in boiling water reactors. Pro Nucl Energ 51: 207-224.
2. Zhilkin AS, Popov EP (2015) Modeling transport of radioactive products of corrosion in loops with sodium coolant. At Energ 119: 37-45.
3. Zhang LF, Chen K, Wang JM, Guo XL, Du DH, et al. (2017) Effects of zinc injection on stress corrosion cracking of cold worked austenitic stainless steel in high-temperature water environments. Scripta Mater 140: 50-54.
4. Ziemniak SE, Hanson M (2006) Zinc treatment effects on corrosion behavior of 304 stainless steel in high temperature, hydrogenated water. Corros Sci 48: 2525-2546.
5. Ohashi T, Ito T, Hosokawa H, Nagase M, Aizawa M (2015) Investigation of cobalt buildup behavior and suppression by zinc injection on stainless steel under hwc conditions using simultaneous continuous measurements of corrosion and cobalt buildup. J Nucl Sci Technol 52: 588-595.
6. Borisevich VD, Pavlov AV, Okhotina IA (2009) Depleted zinc: properties, application, production, Appl Radiat Isot 67: 1167.
7. Honda T, Izumiya M, Matsubayashi H, Ohsumi K, Matsubayashi H (1984) Radiation buildup on stainless steel in a boiling water reactor environment. Nucl Technol 64: 35-42.
8. Castle JE, Masterson HG (1966) The role of diffusion in the oxidation of mild steel in high temperature aqueous solutions. Corros Sci 6: 93-104.
9. Ter-Ovanessian B, Alemany-Dumont C, Normand B (2014) Electronic and transport properties of passive films grown on different Ni-Cr binary alloys in relation to the pitting susceptibility. Electrochim Acta 133: 373-381.
10. Fattah-Alhosseini A, Soltani F, Shirsalimi F, Ezadi B, Attarzadeh N (2011) The semiconducting properties of passive films formed on aisi 316 L and aisi 321 stainless steels: a test of the point defect model (PDM). Corros Sci 53: 3186-3192.
11. Shahryari A, Omanovic S (2007) Improvement of pitting corrosion resistance of a biomedical grade 316LVM stainless steel by electrochemical modification of the passive film semiconducting properties. Electrochem Commun 9: 76-82.
12. Hamadou L, Kadri A, Benbrahim N (2010) Impedance investigation of thermally formed oxide films on aisi 304L stainless steel. Corros Sci 52: 859-864.
13. Taveira LV, Montemor MF, Belo MDC, Ferreira MG, Dick LFP (2010) Influence of incorporated Mo and Nb on the mott–schottky behaviour of anodic films formed on aisi 304L. Corros Sci 52: 2813-2818.
14. Macdonald DD (2011) The history of the point defect model for the passive state: a brief review of film growth aspects, Electrochim Acta 56: 1761-1772.

Author Affiliations Top

School of Environmental Science & Engineering, North China Electric Power University, Baoding 071003, Hebei Province, P. R. China